Journal of Research in Physics Vol. 35, No. 1, 29 - 43 (2011)

doi:10.2478/v10242-012-0003-1

Theoretical Models for Magnetic Properties of Iron Pnictides Part I: Spin Formalism

M. Vujinović, M. Pantić, D. Kapor, S. Radošević
University of Novi Sad, Faculty of Sciences, Department of Physics, Trg Dositeja Obradovića 4, 21000 Novi Sad, Serbia

Received: *December 16, 2011*

Abstract

We attempt to describe the magnetic properties of parent pnictide compounds by using the $J_1 - J_2 - J_c$ Heisenberg model Hamiltonian. In order to obtain the ground state magnetization and spin wave dispersion we use the Green's functions method for spin operators. The equations of motion for Green's functions are decoupled by employing the random phase approximation. We analyze the results numerically and after comparison with experimental data we conclude that the model is to be modified to make it more relevant to iron pnictides.

Key words: Iron pnictides, Green's functions, random phase approximation

1. Introduction

High temperature superconductivity in iron pnictides (more precisely, in iron arsenides) was discovered in the begining of 2008 [1]. This establishes iron pnictides as the second class of materials (first being the copper oxides) that possess superconducting properties at temperatures above 30^o K. There are quite a few analogies between these two classes of high-T_c superconductors. Both iron pnictides and copper oxides possess a layered structure, and it is strongly believed that transition metal layers play a crucial role in the mechanism of high-T_c superconductivity. Also, both classes display a magnetic long-range order which is destroyed by doping when the material goes into the superconducting state [1, 2].

However, at room temperatures, copper oxides are typical insulators while the iron pnictides are bad metals with a small Fermi surface. It seems that both collective and localized magnetic degrees of freedom are important in iron pnictides. This makes the theoretical description of their magnetic properties a significantly greater challenge than for copper oxides. In this paper we attempt to decribe the magnetic properties of iron pnictides by using the picture of well localized electrons, thus ignoring all the collective degrees of freedom. In other words, we use the Heisenberg model [3, 4]. To be more precise, we use the $J_1-J_2-J_c$ Heisenberg model, the details of which are given further in the paper. Our motivation for studying the magnetic properties of iron pnictides stems from the belief

that the magnetism in these materials is closely related to high-T_c superconductivity, just like with the copper oxides.

In order to obtain the magnetisation for the absolute zero temperature and magnon dispersion we use the Green's functions method [5, 6, 7] in two different approaches. In the first approach (presented in this paper) we keep the model Hamiltonian in its original form, meaning that we work with spin operators. The equations of motion for Green's functions in this approach are linearized by means of Tyablikov's decoupling (random phase approximation, RPA) [5]. In the second approach (presented in Part II) we will use the Dyson-Maleev boson representation for spin operators and we will keep only the terms quadratic in Bose-operators, corresponding to Bloch's approximation, or linear spin wave theory (LSW). The results obtained are further investigated numerically. The comparison of numerical simulations with the results of experiments shows that the considered model is applicable only to some extent to undoped iron pnictides. Further work and modifications of the model are required in order to get a better agremeent between the theory and experiment.

2. Iron pnictides in general and the model Hamiltonian

There are three groups of iron arsenides (materials which contain layers of FeAs) [1]. First group contains the materials of the type ReOFeAs, where Re stands for a rare earth element. Members of this group of materials are often referred to as the 1111 type compounds. Low-temeperature superconductivity was first discovered in LaOFeAs, which is a typical member of this group of materials. Critical temperature for these materials can be increased by replacing the oxygen with fluorine, or some other rare earth element. The current 'record holder' for this group and iron pnictides in general is the compound $SmO_{1-x}F_xFeAs$, with $T_c = 55\,\mathrm{K}$. Second group contains compounds of the type AFe_2As_2, with A=Ba,Sr,Ca. These materials are referred to as the 122 type compounds. The third group consists of only one material, LiFeAs, and it is referred to as a 111 type compound.

The experiments of neutron diffraction [8, 9], muon spin resonance [10], and Mossbauer spectroscopy [11] have shown that there exists a long-range magnetic order in the compounds La(Nd)OFeAs and AFe_2As_2. The type of magnetic order is collumnar spin stripe, with alternating collumns of up and down spins. In most cases this magnetic long-range order sets in at temperatures which are the same or slightly lower than the temperatures at which the structural phase transition from tetragonal to orthorombic or monoclinic phase occurs. This closeness of the magnetic and structural phase transitions suggests that there might be some connection between them. However, as the structural phase transition is very small (less than one percent [12]), we shall ignore it in this paper. In other words, we will work with tetragonal lattices only.

Some of the first theoretical results for magnetic properties of iron pnictides were obtained by using LDA (local density approximation) methods. In the LDA approach, the electron correlations are completely ignored. Although this approach was somewhat sucessful, it predicts the values for magnetic momenta which are at least twice larger that those observed in experiments (see Table 1).

Band-structure calculations predict the values for magnetic momenta of up to $2.3\,\mu_B$ per Fe site [19, 20], which is in even worse agreement with experiments. In this paper we take a different route in an attempt to describe the magnetic properties of iron pnictides. There are some experimental results which suggest that iron pnictides are not too far

from being typical Mott-Hubbard insulators. For example, LaOFeAs has a relatively high electric resistance, $\rho \approx 5\,\mathrm{m}\Omega\mathrm{cm}$ [21]. Also, there is no Drude peak in the optical conductivity for this material [22]. On a purely theoretical ground, there are some results which suggest that the Coulomb repulsion on lattice sites should be relatively high for these materials.

Table 1. Comparison of magnetic momenta calculated in LDA approach with those obtained in experiments.

Material	LDA momenta (μ_B) [13]	Exp. momenta (μ_B)
LaOFeAs	1.69	0.36 [14]
NdOFeAs	1.49	0.25 [15]
$CaFe_2As_2$	1.51	0.80 [16]
$BaFe_2As_2$	1.68	0.87 [17]
$SrFe_2As_2$	1.69	1.01 [18]

In the light of these facts, it seems reasonable to treat iron pnictides as pure Mott-Hubbard insulators and to ignore the collective degrees of freedom. We thus adopt a picture of well localized electrons and use the Heisenberg Hamiltonian to describe the dynamics of the system. In order to describe the collumnar spin stripe order found in iron pnictides, we must take into account the nearest-neighbor as well as next-nearest-neighbor interactions in the plane of spin stripes. We would also like to include the nearest-neighbor interactions between the planes of spin stripes.

Our model Hamiltonian thus has the form

$$\hat{H} = J_1 \sum_{\langle \mathbf{i},\mathbf{j} \rangle} \mathbf{S_i} \cdot \mathbf{S_j} + J_2 \sum_{\langle\langle \mathbf{i},\mathbf{j} \rangle\rangle} \mathbf{S_i} \cdot \mathbf{S_j} + J_c \sum_{|\mathbf{i},\mathbf{j}|} \mathbf{S_i} \cdot \mathbf{S_j} \tag{1}$$

Here the sums $\langle \mathbf{i},\mathbf{j} \rangle$ and $\langle\langle \mathbf{i},\mathbf{j} \rangle\rangle$ contain, respectively, nearest-neighbor and next-nearest-neighbor pairs in the plane of spin stripes. The sum $|\mathbf{i},\mathbf{j}|$ contains nearest-neighbor pairs between the planes of spin stripes. The magnetic unit cell and the exchange integrals for interactions we just described are shown in Figure 1.

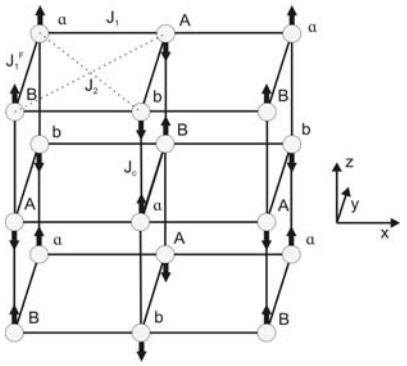

Figure 1. The magnetic unit cell. Four ferromagnetic sublattices are labeled with a, B, A and b. White circles represent Fe^{2+} ions.

Spin stripes lie along the y axis. We introduced two different notations for the NN exchange integral (J_1 and J_1^F) because we want to keep in mind the fact that along the y

axis spins are alligned ferromagnetically, while along the x axis they are alligned antiferromagnetically. The decision on the signs of these exchange integrals will be made when we derive the magnon dispersion law. It should be noted that the ground state of the pure J_1 model has Néel order reduced by quantum fluctuations [4].

We will discuss the parameters of the model (i.e. the exchange integrals J_1, J_2 and J_c) in more detail later. For now it suffices to say that we shall consider only those values for these parameters for which the collumnar spin stripe order is possible. It is well-known that the collumnar spin stripe order can exist for $J_2/J_1 > 0.5$. Also, it must be pointed out that because of the layered structure of iron pnictides the electron states are quasi two-dimensional, with the intraplane interactions much stronger than interplane interactions [1]. This is why we will take the exchange integral J_c to be at least one order of magnitude smaller than the exchange integral J_1.

3. Spin formalism and the RPA approach

In our first attempt to study the dynamics which arises from the model Hamiltonian (1) we shall keep this Hamiltonian in its original form. In other words, we will be working with spin operators. We will use the Green's functions method, which is based on the spectral theorem. We need the equations of motion for Green's functions which contain the operators $\hat{S}^{+}_{\mathbf{n}}(A), \hat{S}^{-}_{\mathbf{n}}(a), \hat{S}^{+}_{\mathbf{n}}(b)$ and $\hat{S}^{-}_{\mathbf{n}}(B)$, because these operators create the excitations in their respective sublattices. Here we give the equations of motion for Green's functions $\langle\langle \hat{S}^{+(A)}_{\mathbf{n}} | \hat{R}_{\mathbf{m}} \rangle\rangle$ and $\langle\langle \hat{S}^{-(a)}_{\mathbf{n}} | \hat{R}_{\mathbf{m}} \rangle\rangle$, while those for $\langle\langle \hat{S}^{+(b)}_{\mathbf{n}} | \hat{R}_{\mathbf{m}} \rangle\rangle$ and $\langle\langle \hat{S}^{-(B)}_{\mathbf{n}} | \hat{R}_{\mathbf{m}} \rangle\rangle$ are very similar:

$$
\begin{aligned}
\omega\langle\langle \hat{S}^{+(A)}_{\mathbf{n}} | \hat{R}_{\mathbf{m}} \rangle\rangle \;=\; & \frac{i}{2\pi}\langle [\hat{S}^{+(A)}_{\mathbf{n}}, \hat{R}_{\mathbf{m}}] \rangle + \\
& + \; J_1 \sum_{\boldsymbol{\delta}^{x}_{Aa}} \langle\langle \hat{S}^{z(A)}_{\mathbf{n}} \hat{S}^{-(a)}_{\mathbf{n}+\boldsymbol{\delta}^{x}_{Aa}} | \hat{R}_{\mathbf{m}} \rangle\rangle + J_1 \sum_{\boldsymbol{\delta}^{x}_{Aa}} \langle\langle \hat{S}^{+(A)}_{\mathbf{n}} \hat{S}^{z(a)}_{\mathbf{n}+\boldsymbol{\delta}^{x}_{Aa}} | \hat{R}_{\mathbf{m}} \rangle\rangle \\
& + \; J_c \sum_{\boldsymbol{\delta}^{z}_{AB}} \langle\langle \hat{S}^{z(A)}_{\mathbf{n}} \hat{S}^{-(B)}_{\mathbf{n}+\boldsymbol{\delta}^{z}_{AB}} | \hat{R}_{\mathbf{m}} \rangle\rangle + J_c \sum_{\boldsymbol{\delta}^{z}_{AB}} \langle\langle \hat{S}^{+(A)}_{\mathbf{n}} \hat{S}^{z(B)}_{\mathbf{n}+\boldsymbol{\delta}^{z}_{AB}} | \hat{R}_{\mathbf{m}} \rangle\rangle \\
& + \; J_1^F \sum_{\boldsymbol{\delta}^{y}_{Ab}} \langle\langle \hat{S}^{z(A)}_{\mathbf{n}} \hat{S}^{+(b)}_{\mathbf{n}+\boldsymbol{\delta}^{y}_{Ab}} | \hat{R}_{\mathbf{m}} \rangle\rangle - J_1^F \sum_{\boldsymbol{\delta}^{y}_{Ab}} \langle\langle \hat{S}^{+(A)}_{\mathbf{n}} \hat{S}^{z(b)}_{\mathbf{n}+\boldsymbol{\delta}^{y}_{Ab}} | \hat{R}_{\mathbf{m}} \rangle\rangle \\
& + \; J_2 \sum_{\boldsymbol{\delta}''_2} \langle\langle \hat{S}^{z(A)}_{\mathbf{n}} \hat{S}^{-(B)}_{\mathbf{n}+\boldsymbol{\delta}''_2} | \hat{R}_{\mathbf{m}} \rangle\rangle + J_2 \sum_{\boldsymbol{\delta}''_2} \langle\langle \hat{S}^{+(A)}_{\mathbf{n}} \hat{S}^{z(B)}_{\mathbf{n}+\boldsymbol{\delta}''_2} | \hat{R}_{\mathbf{m}} \rangle\rangle
\end{aligned}
\tag{2}
$$

$$
\begin{aligned}
\omega\langle\langle \hat{S}^{-(a)}_{\mathbf{n}} | \hat{R}_{\mathbf{m}} \rangle\rangle \;=\; & \frac{i}{2\pi}\langle [\hat{S}^{-(a)}_{\mathbf{n}}, \hat{R}_{\mathbf{m}}] \rangle - \\
& - \; J_1 \sum_{\boldsymbol{\delta}^{x}_{Aa}} \langle\langle \hat{S}^{z(a)}_{\mathbf{n}} \hat{S}^{+(A)}_{\mathbf{n}+\boldsymbol{\delta}^{x}_{Aa}} | \hat{R}_{\mathbf{m}} \rangle\rangle - J_1 \sum_{\boldsymbol{\delta}^{x}_{Aa}} \langle\langle \hat{S}^{-(a)}_{\mathbf{n}} \hat{S}^{z(A)}_{\mathbf{n}+\boldsymbol{\delta}^{x}_{Aa}} | \hat{R}_{\mathbf{m}} \rangle\rangle \\
& - \; J_c \sum_{\boldsymbol{\delta}^{z}_{ab}} \langle\langle \hat{S}^{z(a)}_{\mathbf{n}} \hat{S}^{+(b)}_{\mathbf{n}+\boldsymbol{\delta}^{z}_{ab}} | \hat{R}_{\mathbf{m}} \rangle\rangle - J_c \sum_{\boldsymbol{\delta}^{z}_{ab}} \langle\langle \hat{S}^{-(a)}_{\mathbf{n}} \hat{S}^{z(b)}_{\mathbf{n}+\boldsymbol{\delta}^{z}_{ab}} | \hat{R}_{\mathbf{m}} \rangle\rangle \\
& - \; J_1^F \sum_{\boldsymbol{\delta}^{y}_{aB}} \langle\langle \hat{S}^{z(a)}_{\mathbf{n}} \hat{S}^{-(B)}_{\mathbf{n}+\boldsymbol{\delta}^{y}_{aB}} | \hat{R}_{\mathbf{m}} \rangle\rangle + J_1^F \sum_{\boldsymbol{\delta}^{y}_{aB}} \langle\langle \hat{S}^{-(a)}_{\mathbf{n}} \hat{S}^{z(B)}_{\mathbf{n}+\boldsymbol{\delta}^{y}_{aB}} | \hat{R}_{\mathbf{m}} \rangle\rangle \\
& - \; J_2 \sum_{\boldsymbol{\delta}''_2} \langle\langle \hat{S}^{z(a)}_{\mathbf{n}} \hat{S}^{+(b)}_{\mathbf{n}+\boldsymbol{\delta}''_2} | \hat{R}_{\mathbf{m}} \rangle\rangle - J_2 \sum_{\boldsymbol{\delta}''_2} \langle\langle \hat{S}^{-(a)}_{\mathbf{n}} \hat{S}^{z(b)}_{\mathbf{n}+\boldsymbol{\delta}''_2} | \hat{R}_{\mathbf{m}} \rangle\rangle
\end{aligned}
\tag{3}
$$

Here $\hat{R}_{\mathbf{m}}$ is an arbitrary operator which we shall choose later. It is obvious that equations (2) and (3) are nonlinear, and the same is true for the equations of motion for $\langle\langle \hat{S}^{+(b)}_{\mathbf{n}} | \hat{R}_{\mathbf{m}} \rangle\rangle$ and $\langle\langle \hat{S}^{-(B)}_{\mathbf{n}} | \hat{R}_{\mathbf{m}} \rangle\rangle$. In order to linearize these equations of motion we employ the random phase approximation. Further simplification of the equations of motion follows after the Fourier transformation into the momentum space:

$$\langle\langle \hat{S}^{\pm}_{\mathbf{n}} | \hat{R}_{\mathbf{m}} \rangle\rangle = \frac{1}{N} \sum_{\mathbf{k}} \langle\langle \hat{S}^{\pm} | \hat{R} \rangle\rangle_{\mathbf{k}} e^{i\mathbf{k}\cdot(\mathbf{n}-\mathbf{m})} \tag{4}$$

Components of the wave vector $\mathbf{k}$ lie within the first Brillouin zone:

$$k_x = (-\frac{\pi}{2a}, \frac{\pi}{2a}), \quad k_y = (-\frac{\pi}{a}, \frac{\pi}{a}), \quad k_z = (-\frac{\pi}{2c}, \frac{\pi}{2c}) \tag{5}$$

a and c are parameters of the (tetragonal) lattice in direct space. The system of equations of motion becomes:

$$(\omega-\varepsilon)\langle\langle \hat{S}^{+(A)} | \hat{R} \rangle\rangle - J_x \langle\langle \hat{S}^{-(a)} | \hat{R} \rangle\rangle - J_y \langle\langle \hat{S}^{+(b)} | \hat{R} \rangle\rangle - J_{2c} \langle\langle \hat{S}^{-(B)} | \hat{R} \rangle\rangle = \frac{i}{2\pi} \langle [\hat{S}^{+(A)}, \hat{R}] \rangle \tag{6a}$$

$$J_x \langle\langle \hat{S}^{+(A)} | \hat{R} \rangle\rangle + (\omega+\varepsilon)\langle\langle \hat{S}^{-(a)} | \hat{R} \rangle\rangle + J_{2c} \langle\langle \hat{S}^{+(b)} | \hat{R} \rangle\rangle + J_y \langle\langle \hat{S}^{-(B)} | \hat{R} \rangle\rangle = \frac{i}{2\pi} \langle [\hat{S}^{-(a)}, \hat{R}] \rangle \tag{6b}$$

$$-J_y \langle\langle \hat{S}^{+(A)} | \hat{R} \rangle\rangle - J_{2c} \langle\langle \hat{S}^{-(a)} | \hat{R} \rangle\rangle + (\omega+\varepsilon)\langle\langle \hat{S}^{+(b)} | \hat{R} \rangle\rangle - J_x \langle\langle \hat{S}^{-(B)} | \hat{R} \rangle\rangle = \frac{i}{2\pi} \langle [\hat{S}^{+(b)}, \hat{R}] \rangle \tag{6c}$$

$$J_{2c} \langle\langle \hat{S}^{+(A)} | \hat{R} \rangle\rangle + J_y \langle\langle \hat{S}^{-(a)} | \hat{R} \rangle\rangle + J_x \langle\langle \hat{S}^{+(b)} | \hat{R} \rangle\rangle + (\omega+\varepsilon)\langle\langle \hat{S}^{-(B)} | \hat{R} \rangle\rangle = \frac{i}{2\pi} \langle [\hat{S}^{-(B)}, \hat{R}] \rangle \tag{6d}$$

We introduced the following notation for geometric factors:

$$\varepsilon = 2\sigma(J_1 + J_c - J_1^F + 2J_2) \tag{7}$$

$$J_x = 2\sigma J_1 \cos ak_x \ , \ J_y = 2\sigma J_1^F \cos ak_y \tag{8}$$

$$J_{2c} = 2\sigma\Big(2J_2\gamma_2(\mathbf{k}_{||}) + J_c \cos ck_z\Big), \quad \gamma_2(\mathbf{k}_{||}) = \cos ak_x \cos ak_y \tag{9}$$

Here $\langle \hat{S}^z_{\mathbf{n}} \rangle = \sigma$ is an order parameter, the magnetization of one sublattice. We assumed that the average magnetization is the same for all lattice sites. Equations (6a)-(6d) form a closed inhomogeneous system for Fourier images of Green's functions. The determinant of the system is given by:

$$\Delta_4(\omega) = \begin{vmatrix} \omega-\varepsilon & -J_x & -J_y & -J_{2c} \\ J_x & \omega+\varepsilon & J_{2c} & J_y \\ -J_y & -J_{2c} & \omega-\varepsilon & -J_x \\ J_{2c} & J_y & J_x & \omega+\varepsilon \end{vmatrix} \tag{10}$$

The equation $\Delta_4(\omega) = 0$ gives us the magnon dispersion law. For the NN exchange integrals we choose $J_1 = J_1^F$ so that the stripe order is completely spontaneous. With this choice the four energy branches of magnetic excitations have the following form:

$$E_1 = 2\sigma\sqrt{J_c(1+\cos ck_z) + 2J_2(1+\gamma_2(\mathbf{k}_{||})) - J_1(\cos ak_x + \cos ak_y)} \times \\ \times \sqrt{J_c(1-\cos ck_z) + 2J_2(1-\gamma_2(\mathbf{k}_{||})) + J_1(\cos ak_x - \cos ak_y)} \tag{11}$$

$$E_2 = 2\sigma\sqrt{J_c(1+\cos ck_z) + 2J_2(1+\gamma_2(\mathbf{k}_{||})) + J_1(\cos ak_x + \cos ak_y)} \times \\ \times \sqrt{J_c(1-\cos ck_z) + 2J_2(1-\gamma_2(\mathbf{k}_{||})) - J_1(\cos ak_x - \cos ak_y)} \tag{12}$$

$$E_3 = -E_1 \tag{13}$$

$$E_4 = -E_2 \tag{14}$$

We would like to point out that the branches E_1 and E_2 can be interchanged with the substitution $J_1 \to -J_1$ ($E_1(-J_1) = E_2(J_1)$ and vice versa). Aside from the magnon dispersion, we also need to find the average magnetization, which we assumed to be the same for all sublattices. In order to find the desired magnetization we first calculate the correlation function $\langle \hat{S}^-(A)\hat{S}^+(A)\rangle$ by employing the spectral theorem. One can calculate $\langle \hat{S}^-(A)\hat{S}^+(A)\rangle$ if one knows the Green's function $\langle\langle \hat{S}^+(A)|\hat{S}^-(A)\rangle\rangle_{\omega,\mathbf{k}}$. This Green's function can be calculated from the system of equations (6a)-(6d). For the operator $\hat{R}$ we choose $\hat{R} = \hat{S}^-(A)$. From the commutation relations for spin operators and Kramer's rule it follows that $\langle\langle \hat{S}^+(A)|\hat{S}^-(A)\rangle\rangle_{\omega,\mathbf{k}}$ is given by:

$$\langle\langle \hat{S}^+(A)|\hat{S}^-(A)\rangle\rangle_{\omega,\mathbf{k}} = \frac{i}{2\pi}\frac{P_3(E)}{\Delta_4(E)} \tag{15}$$

We work in the system of units where $\hbar = 1$ holds, so $\omega = E$. $P_3(E)$ is the determinant for $\langle\langle \hat{S}^+(A)|\hat{S}^-(A)\rangle\rangle_{\omega,\mathbf{k}}$:

$$P_3(E) = \begin{vmatrix} 2\sigma & -J_x & -J_y & -J_{2c} \\ 0 & E+\varepsilon & J_{2c} & J_y \\ 0 & -J_{2c} & E-\varepsilon & -J_x \\ 0 & J_y & J_x & E+\varepsilon \end{vmatrix} \tag{16}$$

$$P_3(E) = 2\sigma\Big[(E+\varepsilon+J_y)(J_y-\varepsilon-E)(\varepsilon-E) + (E+\varepsilon)(J_x^2+J_{2c}^2) - 2J_xJ_yJ_{2c}\Big] \tag{17}$$

We would like to point out that if we wanted to find the magnetization for some other sublattice (by choosing the operator $\hat{R}$ appropriately), we would get the determinant for Green's function which is identical to (17), with only a change in the sign of energy $E \to -E$ in some cases. This change in the sign of energy is irrelevant because, as we shall show, the final expression for the correlation function is independent of the sign of energy (it is an even function of energy). This fact justifies our previous assumption that the average magnetization is the same for all sublattices. The expression (15) for the Green's function can be put in a simpler form:

$$\langle\langle \hat{S}^+(A)|\hat{S}^-(A)\rangle\rangle_{\omega,\mathbf{k}} = \frac{i}{2\pi}\Big[\frac{K(E_1)}{E-E_1} + \frac{K(-E_1)}{E+E_1} + \frac{K(E_2)}{E-E_1} + \frac{K(-E_2)}{E+E_2}\Big] \tag{18}$$

Here the coefficients $K(E_i)$ are given by [23]:

$$K(E_i) = \frac{P_3(E_i)}{\frac{d}{dE}\Delta_4(E)_{|_{E=E_i}}} = \frac{P_3(E_i)}{2E_i(2E_i^2 - E_1^2 - E_2^2)} \tag{19}$$

By performing the inverse Fourier transform we get:

$$\langle \hat{S}^-_{\mathbf{m}}(A)\hat{S}^+_{\mathbf{n}}(A)\rangle = \frac{1}{N}\sum_{\mathbf{k}}\int_{-\infty}^{+\infty} d\omega I_{\hat{S}^-\hat{S}^+}(\mathbf{k},\omega)e^{-i\mathbf{k}\cdot(\mathbf{n}-\mathbf{m})} \tag{20}$$

The spectral intensity $I_{\hat{S}^-\hat{S}^+}$ is given by:

$$\begin{aligned} I_{\hat{S}^-\hat{S}^+} = {} & 2\sigma\Big[\frac{K(E_1)}{e^{E/T}-1}\delta(E-E_1) + \frac{K(-E_1)}{e^{E/T}-1}\delta(E+E_1) + \frac{K(E_2)}{e^{E/T}-1}\delta(E-E_2) + \\ & + \frac{K(-E_2)}{e^{E/T}-1}\delta(E+E_2)\Big] \end{aligned} \tag{21}$$

With the choice $\mathbf{n} = \mathbf{m}$ we get for the correlation function:

$$\langle \hat{S}^-_{\mathbf{n}}(A)\hat{S}^+_{\mathbf{n}}(A)\rangle = \frac{2\sigma}{N}\sum_{\mathbf{k}}\Big[\frac{K(E_1)}{e^{E_1/T}-1}+\frac{K(-E_1)}{e^{-E_1/T}-1}+\frac{K(E_2)}{e^{E_2/T}-1}+\frac{K(-E_2)}{e^{-E_2/T}-1}\Big] \tag{22}$$

After some lenghty but straightforward calculations we obtain the final expression for the correlation function for an arbitrary temperature:

$$\langle \hat{S}^-_{\mathbf{n}}(A)\hat{S}^+_{\mathbf{n}}(A)\rangle = 2\sigma P_S(T) \tag{23}$$

$$P_S(T) = \frac{1}{4N}\sum_{\mathbf{k}}\Big[\frac{\varepsilon - J_y}{E_1}\coth\frac{E_1}{2T}+\frac{\varepsilon+J_y}{E_2}\coth\frac{E_2}{2T}\Big]-\frac{1}{2} \tag{24}$$

Thus the correlation function is an even function of energy. We are only interested in the results for absolute zero temperature:

$$\begin{aligned} P_S(0) &= \frac{1}{4N}\sum_{\mathbf{k}}\Big(\frac{\varepsilon-J_y}{E_1}+\frac{\varepsilon+J_y}{E_2}\Big)-\frac{1}{2} \\ &= \frac{1}{4N}\sum_{\mathbf{k}}\Big(\frac{Y+2-X\cos ak_y}{\sqrt{\cdots}_1}+\frac{Y+2+X\cos ak_y}{\sqrt{\cdots}_2}\Big)-\frac{1}{2} \end{aligned} \tag{25}$$

Here we introduced the notation:

$$X = J_1/J_2\ , \quad Y = J_c/J_2 \tag{26}$$

$$\begin{aligned} \sqrt{\cdots}_1 &= \sqrt{Y(1-\cos ck_z)+X(\cos ak_x-\cos ak_y)+2(1-\gamma_2(\mathbf{k}_{||}))}\times \\ &\times\ \sqrt{Y(1+\cos ck_z)-X(\cos ak_x+\cos ak_y)+2(1+\gamma_2(\mathbf{k}_{||}))} \end{aligned} \tag{27}$$

$$\begin{aligned} \sqrt{\cdots}_2 &= \sqrt{Y(1-\cos ck_z)-X(\cos ak_x-\cos ak_y)+2(1-\gamma_2(\mathbf{k}_{||}))}\times \\ &\times\ \sqrt{Y(1+\cos ck_z)+X(\cos ak_x+\cos ak_y)+2(1+\gamma_2(\mathbf{k}_{||}))} \end{aligned} \tag{28}$$

In this way $P_S(0)$ is expressed as a function of the so-called frustration parameters $X = J_1/J_2$ and $Y = J_c/J_2$. One last step before finding the expressions for average magnetization is going from summation to integration in the first Brillouin zone:

$$\frac{1}{N}\sum_{\mathbf{k}}(\ldots) \longrightarrow \frac{4}{\pi^3}\int_0^{\pi/2}dx\int_0^{\pi}dy\int_0^{\pi/2}dz(\ldots) \tag{29}$$

Here $x = ak_x, y = ak_y, z = ck_z$. To find the average magnetization σ from P_S, we use the Callen's expression [24]:

$$\sigma = \frac{(S-P_S)(1+P_S)^{2S+1}+(1+S+P_S)P_S^{2S+1}}{(1+P_S)^{2S+1}-P_S^{2S+1}} \tag{30}$$

Finally, for spins 1/2 and 1, we find:

$$\sigma(0) = I^{-1}\ , \quad S = 1/2 \tag{31}$$

$$\sigma(0) = \frac{2I}{1 + \frac{3}{4}I^2} \ , \quad S = 1 \tag{32}$$

$$I = \frac{4}{\pi^3} \int_0^{\pi/2} dx \int_0^{\pi} dy \int_0^{\pi/2} dz \Big(\frac{Y + 2 - X\cos y}{\sqrt{\cdots}_1} + \frac{Y + 2 + X\cos y}{\sqrt{\cdots}_2} \Big) \tag{33}$$

It should be clear that the integral I cannot be handled analytically. We will use numerical methods to further analyze the magnetization and the dispersion law.

4. Numerical calculations and comparison with experiments

We obtained the analytical expressions for zero temperature sublattice magnetization for spins $S = 1/2$ and $S = 1$ (eqs. (31) and (32) respectively). The graphs of these functions are shown in Figure 2.

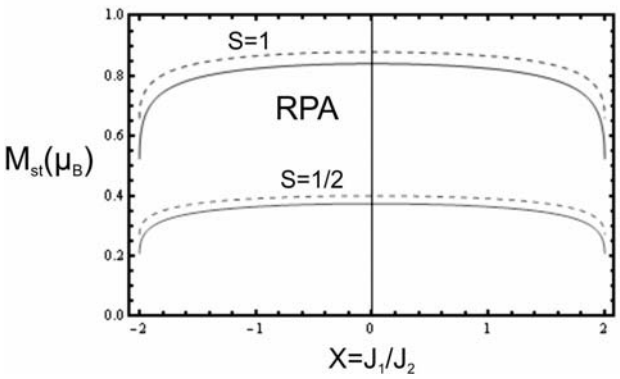

Figure 2. Magnetization as a function of the frustration parameter $X = J_1/J_2$ in the RPA approach. Full-line curves correspond to the value of the parameter $Y = 0.01$, dashed-line curves correspond to the value $Y = 0.1$. .

The first thing one notices about these graphs is that the curves for spins $S = 1/2$ and $S = 1$ are remarkably similar, they are qualitatively the same.

The influence of quantum fluctuations is also evident in these graphs. Classically, we would expect $\langle \hat{S}^z \rangle = S$ to hold for zero temperature, but we see that $\langle \hat{S}^z \rangle$ is always smaller than S. In order to fully appreciate the information that graphs in Figure 2 give us, we must know something about the results of the purely two-dimensional $J_1 - J_2$ model. In the $J_1 - J_2$ model quantum fluctuations are logarithmically divergent, meaning that for all values of spin S magnetization curves go to 0 when $|X| \to 2$ [25]. We see that this is not true in the three-dimensional model. For large enough interplanar coupling (i.e. large enough $Y = J_c/J_2$) the magnetization has a finite value for $|X| = 2$. Thus the interplanar coupling strengthens the magnetization.

We can compare the results shown in Figure 2 with the experimental values for magnetization given in Table 1. It is not yet clear what spin quantum number should be used for iron pnictides. Band structure calculations predict that there can be up to two electrons alligned on one lattice site [19, 26]. There are also some theoretical results which suggest that $S = 1$ is the appropriate choice for iron pnictides [27]. We thus compare the

$S = 1$ curves with the experimental data in Table 1. We see that for 122 type compounds the results are relatively satisfactory, because for a wide range of the parameter X the theoretical values are close to experimental ones. However, for the 1111 type compounds the results are not satisfactory. For $S = 1$ and $|X| = 2$ the magnetization has a finite value which is too high compared to the local magnetic momenta observed in the 1111 type compounds. This statement is true for both values of the parameter Y which we considered ($Y = 0.01$ and $Y = 0.1$).

The disagreement between the theory and experiments for sublattice magnetization should not discourage us, because it does not mean that the model Hamiltonian (1) is inapplicable to iron pnictides. The staggered magnetization may depend on additional collective degrees of freedom, hybridization, and so on. The dispersion law, on the other hand, depends only on the model Hamiltonian, and it is thus a better test for the applicability of the model.

In Figure 3 we show the graphs for the branches E_1 and E_2, as functions of the variables $x = ak_x, y = ak_y, z = ck_z$. We would like to point out that in Ref. [28], which was the basic motivation for our work, there is no branch E_1. The origin of this discrepancy is unknown to us. It may lie in the fact that direct diagonalization (via Bogoliubov transformation) of the Hamiltonian was employed in that paper, while we used the Green's functions method.

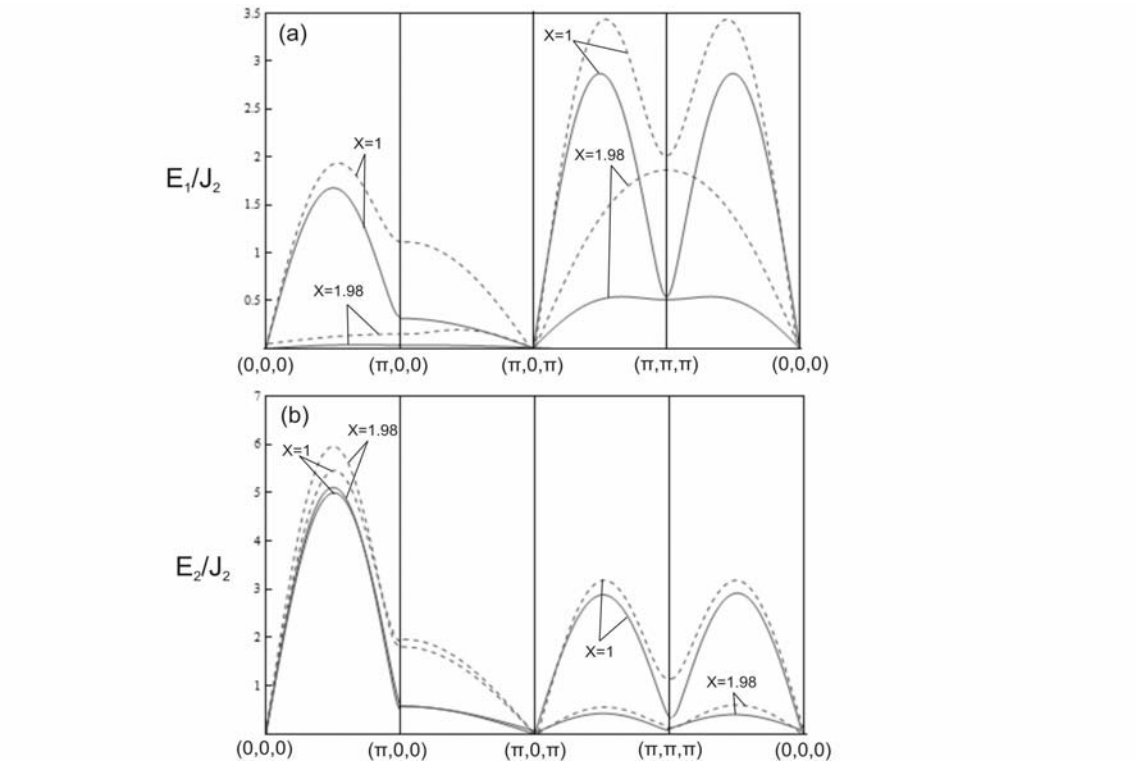

Figure 3. Magnon dispersion branches E_1 and E_2 in RPA theory. Full-line curves correspond to the value of the parameter $Y{=}0.01$, dashed-line curves correspond to the value $Y{=}0.1$. Notice that the two branches have the same Goldstone modes.

We see that the branches E_1 and E_2 have the same Goldstone modes. These are symmetry related modes at $(0, 0, 0)$ and $(\pi, 0, \pi)$. We can obtain the velocities of spin

waves along three axes of the crystal lattice by Taylor expanding the expressions for E_1 and E_2 around either $(0,0,0)$ or $(\pi,0,\pi)$. By discarding terms of the form x^4, x^2y^2 etc. we obtain for the Goldstone mode excitations:

$$E/J_2 \sim \sqrt{v_{x_r}^2(ak_x)^2 + v_{y_r}^2(ak_y)^2 + v_{z_r}^2(ck_z)^2} \tag{34}$$

For the branch E_1 the 'reduced' velocities $v_{x_r}, v_{y_r}, v_{z_r}$ are given by:

$$v_{x_r} = \frac{v_x}{J_2} = 2\sigma\sqrt{(2-X)(2-X+Y)} \tag{35}$$

$$v_{y_r} = \frac{v_y}{J_2} = 2\sigma\sqrt{(2+X)(2-X+Y)} \tag{36}$$

$$v_{z_r} = \frac{v_z}{J_2} = 2\sigma\sqrt{Y(2-X+Y)} \tag{37}$$

From these expressions we can obtain the corresponding results for E_2 by substituting $X \to -X$:

$$\frac{v_x}{J_2} = 2\sigma\sqrt{(2+X)(2+X+Y)} \tag{38}$$

$$\frac{v_y}{J_2} = 2\sigma\sqrt{(2-X)(2+X+Y)} \tag{39}$$

$$\frac{v_x}{J_2} = 2\sigma\sqrt{Y(2+X+Y)} \tag{40}$$

The expressions for spin-wave velocities along the crystal lattice axes and the results we obtained for average magnetization tell us that there exists a somewhat exotic kind of instability of the collumnar spin stripe phase in three dimensions. For small enough interplanar coupling (small enough Y) the average magnetization goes to 0 when $X \to 0$, and the velocities of spin waves vanish as well. This is the 'standard' instability of the spin stripe phase. However, for large values of the parameter Y, magnetization stays finite when $X = 2$, but we see from the equations (35)-(40) that one of the spin-wave velocities must vanish (v_x for the excitation branch E_1, v_y for the branch E_2). Thus, for a large enough Y, the long-range magnetic order survives for $X = 2$, but the spin-stripe phase does not. The nature of the long-range order that sets in for $X = 2$ is unknown to us.

From now on we will mostly be working with the branch E_2 and the corresponding Goldstone mode. Analogous results for the branch E_1 can be easily obtained with the substitution $X \to -X$. From (38) and (39) we see that the ratio v_y/v_x depends strongly on the parameter X:

$$\frac{v_y}{v_x} = \frac{v_{y_r}}{v_{x_r}} = \sqrt{\frac{2-X}{2+X}} \tag{41}$$

For the branch E_1, a reciprocal relation holds. Spin-wave velocities along the x and z axes were measured in neutron diffraction experiments for $SrFe_2As_2$ [29] and $BaFe_2As_2$ [30]. The results are $v_x \approx 205$ meV and $v_z \approx 45$ meV. In order to compare our results for spin-wave velocities with experiments we need at least an estimate for the exchange integral J_2. Some band structure calculations give an estimate $J_2 = 33$ meV [31]. If we accept this result we see in Figure 4 that the velocities v_x and v_z for the branch E_2 and spin $S = 1$ are not far away from experimental results for most values of the parameter X.

Unfortunately, measurement of the velocity v_y has so far proven to be considerably more challenging and there is no universal agreement on its estimated value. Neutron diffraction experiments suggest that the value for v_y is close to v_x [9], while NMR results imply that v_y is an order of magnitude smaller than v_x, with the value estimated to be between 10 and 30 meV [32]. From Figure 4 and the equation (41) we see that in our model v_y can be an order of magnitude smaller than v_x only if $X \approx 2$.

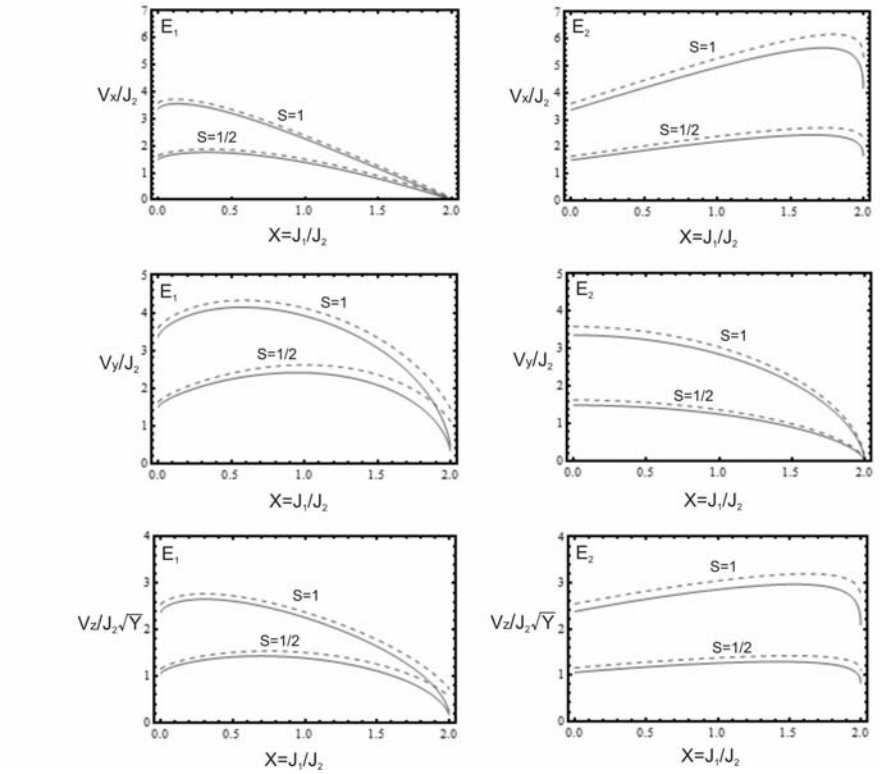

Figure 4. Velocities of spin waves along crystal axes for the branches E_1 (left) and E_2 (right). Full-line curves correspond to the value of the parameter $Y=0.01$, dashed-line curves correspond to the value $Y=0.1$.

Because of this uncertainty for the velocity v_y we must take into consideration both estimates, one from the neutron diffraction, and the other from nuclear magnetic resonance. For NMR estimate we take $v_y/v_x = 0.1$, and from equation (41) we get $X = 1.96$. For neutron diffraction estimate we take $v_y/v_x = 0.7$ and from (41) we get $X = 0.7$. For the branch E_1 the corresponding results would be $X = -1.96$ and $X = -0.7$.

In Figure 5 we show the spin wave dispersion in the x, y plane for two values of X, 1.96 and 0.7. Spin wave dispersion in the y, z plane is shown in Figure 6 for the same values of X. Dispersion in the y, z is useful because it shows the effect of the interplanar coupling and how far the spin waves propagate along the z axis. It also presents a way to determine whether quantum fluctuations persist in three dimensions. Of course, the graphs in Figures 5 and 6 give only a qualitative overview.

A quantitative comparison between the theoretical magnon dispersion and experiments is given in Figure 7. Black dots in Figure 7 represent the experimental data obtained via

inelastic neutron diffraction on $CaFe_2As_2$. Experimental data were taken from Ref. [9]. To convert the theoretical dispersion from the 'unit' J_2 to meVs an estimate $J_2 \approx 33\,\text{meV}$ from band structure calculations was used. We see that essentially all curves in Figure 7(a) follow the experimental data with tolerable deviations.

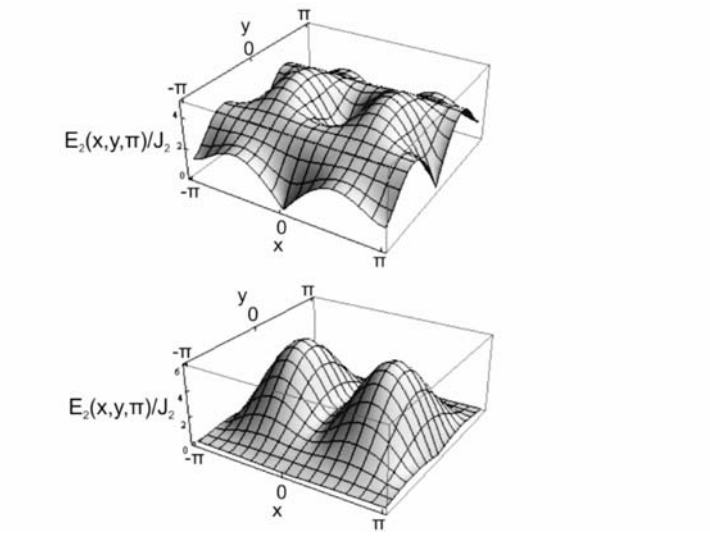

Figure 5. Spin-wave dispersion in the x, y plane for $X = 0.7$ (up) and $X = 1.96$ (down). Only results for spin $S = 1$ and $Y = 0.1$ are shown. .

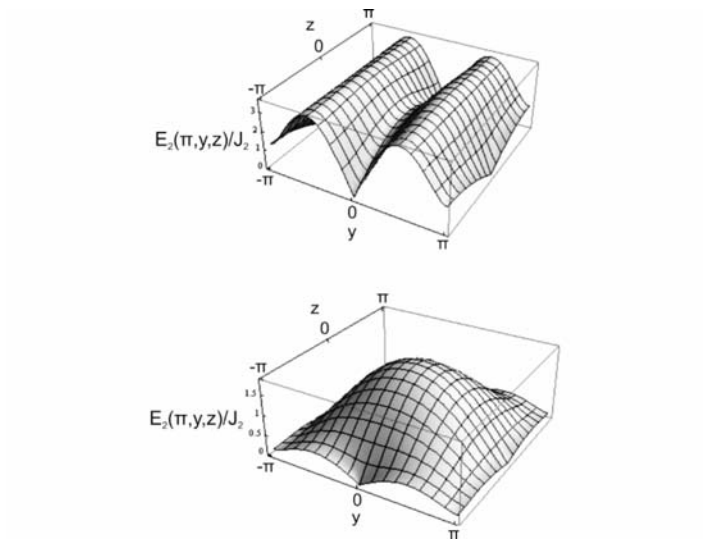

Figure 6. Spin-wave dispersion in the y, z plane for $X = 0.7$ (up) and $X = 1.96$ (down). Only results for spin $S = 1$ and $Y = 0.1$ are shown. .

However, the graphs in Figure 7(b) remove all doubt about the applicability of our model to iron pnictides. We see that dashed-line curves (corresponding to the value $X = 1.96$) do not follow the experimental data even slightly. This suggests that iron pnictides are deep

in the collumnar spin stripe phase, with $X \approx 1$. This conclusion is in agreement with band structure calculations. Unfortunately, it is obvious that the curves for $X = 0.7$ follow the experimental data only to some extent, and that here too there are large deviations between theory and experiment. Thus, if we choose the value of the parameter X in accordance with the results of neutron diffraction experiments, we get the spin wave dispersion that does not match the neutron diffraction data globally. We are finally led to a conclusion that the isotropic $J_1 - J_2 - J_c$ Heisenberg model is not fully applicable to iron pnictides and that modifications are required.

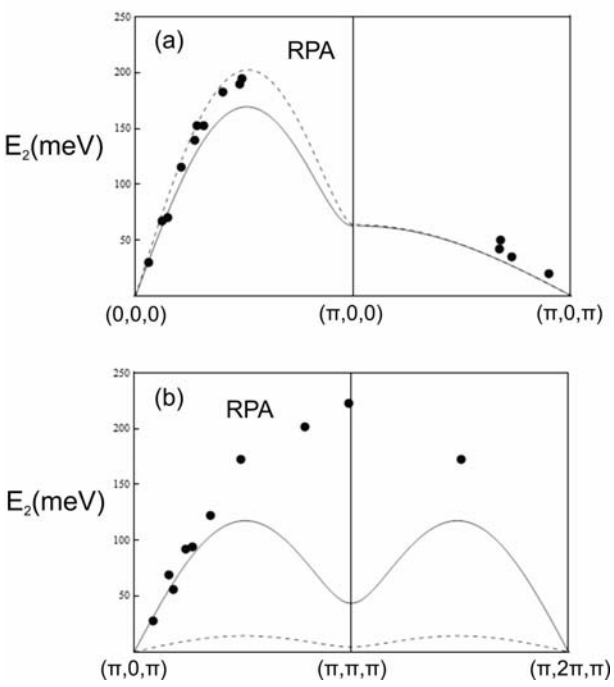

Figure 7. Comparison between the theory and experiment for spin wave dispersion in RPA. Full-line curves correspond to the value of the parameter $X = 0.7$, dashed-line curves correspond to the value $X = 1.96$. All theoretical results are for $Y = 0.1$.

5. Conclusion

In this paper we studied the dispersion law and the ground state magnetization of the $J_1 - J_2 - J_c$ Heisenberg model and checked the relevance of the model to undoped iron pnictides. We obtained the dispersion law and the staggered magnetization from the model Hamiltonian by using the Green's function method. Here we used the spin formalism in random phase approximation. Analogous results for LSW will be shown in Part II. The results for the average magnetization agree fairly nicely with measured values for the 122 type compounds, but for the 1111 type compounds there is great disagreement between theory and experiment. This does not mean that the model is irrelevant for iron pnictides, because the magnetization may depend on additional factors that are hard to account for.

This is why we turned to the dispersion law, as it depends only on the model Hamiltonian. We found two distinct energy branches and showed that they posses the same

Goldstone modes. Through a standard procedure we found the velocities of the Goldstone mode excitations. The ratio of velocities along the x and y axes depends strongly on the parameter $X = J_1/J_2$, so we used the experimental data for these velocities to obtain an estimate for X. There is no an universal agreement about the value of the velocity v_y, so we had to consider two values for X. For neither of these two values did we get the theoretical dispersion to match the measured one globally. We were led to a conclusion that the considered model is not completely relevant to undoped pnictides and that modifications are required.

Acknowledgments

This work was supported by the Serbian Ministry of Education and Science, Project No. OI 171009.

References

[1] Y. Izyumov, E. Kurmaev, *High-Tc. Superconductors Based on FeAs Compounds*, (Springer-Verlag, Berlin Heidelberg, 2010).

[2] M. A. Kastner, R. J. Birgeneau, G. Shirane, Y. Endoh, Rev. Mod. Phys. **70**, 897 (1998).

[3] K. Yosida, *Theory of Magnetisam*, (Springer-Verlag, New York, 1991).

[4] E. Manousakis, Rev. Mod. Phys. **63** 1 (1991).

[5] S. V. Tyablikov, *The Methods in the Quantum Theory of Magnetism*, (Plenum Press, 1967).

[6] W. Nolting, A. Ramakanth, *Quantum Theory of Magnetism*, (Springer-Verlag, Berlin Heidelberg, 2009).

[7] B. S. Tošić, *Statistička fizika*, (PMF u Novom Sadu, Novi Sad, 1978),
M. Pantić, *Predavanja iz statističke fizike* (lecture notes), Novi Sad, 2009

[8] C. de la Cruz, Q. Huang, J. W. Lynn, J. Li, W. Ratcliff II, J. L. Zaretsky, H. A. Mook, G. F. Chen, J. L. Luo, N. L. Wang, P. Dai, Nat. Lett. **453**, 07057 (2008).

[9] J. Zhao, D. T. Adroja, D.-X. Yao, R. Bewley, S. Li, X. F. Wang, G. Wu, X. H. Chen, J. Hu, P. Dai, Nat. Phys. **5**, 555 (2009).

[10] A. J. Drew, F. L. Pratt, T. Lancaster, S. J. Blundell, P. J. Baker, R. H. Liu, G. Wu, X. H. Chen, I. Watanabe, V. K. Malik *et al.* Phys. Rev. Lett. **101**, 097010 (2008).

[11] H. Leutkens, H.-H. Klauss, M. Kraken, F. J. Litterst, T. Dellmann, R. Klingeler, C. Hess, R. Khasanov, A. Amato, C. Baines *et al.*, Nat. Mat. **8**, 305 (2009).

[12] J. Zhao, Q. Huang, C. de la Cruz, S.Li, J. W. Lynn, Y. Chen, M. A. Green, G. F. Chen, G. Li, Z.Li, J. L. Luo, N. L. Wang and P.Dai, Nat. Mat. **7**, 953 (2008).

[13] M. J. Han, Q. Yin, W. E. Pickett, S. Y. Savrasov, Phys. Rev. Lett. **102** 107003 (2009).

[14] C. de la Cruz, Q. Huang, J. W. Lynn, J. Li, W. Ratcliff II, J. L. Zaretsky, H. A. Mook, G. F. Chen, J. L. Luo, N. L. Wang *et al.*, Nature, **453**, 899 (2008).

[15] Y. Chen, J.W. Lynn, J. Li, G. Li, G. F. Chen, J. L. Luo, N. L. Wang, P. Dai, C. de la Cruz, and H. A. Mook, Phys. Rev. B **78**, 064515 (2008).

[16] S. O. Diallo, V. P. Antropov, T. G. Perring, C. Broholm, J. J. Pulikkotil, N. Ni, S. L. Budko, P. C. Canfield, A. Kreyssig, A. I. Goldman *et al.*, Phys. Rev. Lett. **102**, 187206 (2009).

[17] Q. Huang, Y. Qiu, W. Bao, M. A. Green, J. W. Lynn, Y. C. Gasparovic, T. Wu, G. Wu, and X. H. Chen, Phys. Rev. Lett. **101**, 257003 (2008).

[18] K. Kaneko, A. Hoser, N. Caroca-Canales, A. Jesche, C. Krellner, O. Stockert, and C. Geibel, Phys. Rev. B **78**, 212502 (2008).

[19] Z. P. Yin, S. Lebeque, M. J. Han, B. P. Neal, S. Y. Savrasov, W. E. Picket, Phys. Rev. Lett. **101**, 047001 (2008).

[20] F. Ma, W. Ji, J. Hu Z.-Y. Lu, T. Xiang, Phys. Rev. Lett. **102**, 177003 (2009).

[21] Q. Si, E. Abrahams, Phys. Rev. Lett. **101**, 076401 (2008).

[22] J. Dong *et al.* Europhys. Lett. **83**, 27006 (2008).

[23] I. N. Bronshtein, K. A. Semendyayev, G. Musiol, H. Muehliq, H. Muhliq, *Handbook of Mathematics*, (Springer, 2004)

[24] H.B. Callen, Phys. Rev. **130**, 890 (1963).

[25] G. S. Uhrig, M. Holt, J. Oitmaa, O. P. Sushkov, R. P. Singh, Phys. Rev. B **79**, 092416 (2009).

[26] F. Ma, Z.-Y. Lu, Phys. Rev. B **78**, 033111 (2008).

[27] M. M. Korshunov, I. Eremin, Phys. Rev. B **78**, 140509(R) (2008).

[28] M. Holt, O. P. Sushkov, D. Stanek, G.S. Uhrig, Phys. Rev. B **83**, 144528 (2011).

[29] J. Zhao, D.-X. Yao, S. Li, T. Hong, Y. Chen, S. Chang, W. R. II, J. W. Lynn, H. A. Mook, G. F. Chen *et al.*, Phys. Rev. Lett. **101**, 167203 (2008).

[30] R. A. Ewings, T. G. Perring, R. I. Bewley, T. Guidi, M. J. Pitcher, D. R. Parker, S. J. Clarke, and A. T. Boothroyd, Phys. Rev. B **78**, 220501(R) (2008).

[31] T. Yildirim, Phys. Rev. Lett. **101**, 057010 (2008).

[32] A. Ong, G. S. Uhrig, O. P. Sushkov, Phys. Rev. B **80**, 014514 (2009).